Mechanics model for actin-based motility

Yuan Lin
Department of Mechanical Engineering, The University of Hong Kong, Hong Kong SAR, China
(Received 10 November 2008; revised manuscript received 29 December 2008; published 26 February 2009)

We present here a mechanics model for the force generation by actin polymerization. The possible adhesions between the actin filaments and the load surface, as well as the nucleation and capping of filament tips, are included in this model on top of the well-known elastic Brownian ratchet formulation. A closed form solution is provided from which the force-velocity relationship, summarizing the mechanics of polymerization, can be drawn. Model predictions on the velocity of moving beads driven by actin polymerization are consistent with experiment observations. This model also seems capable of explaining the enhanced actin-based motility of Listeria monocytogenes and beads by the presence of Vasodilator-stimulated phosphoprotein, as observed in recent experiments.

DOI: 10.1103/PhysRevE.79.021916 PACS number(s): 87.10.−e, 87.17.Aa, 87.17.Jj

I. INTRODUCTION

The motility of certain pathogens, such as Listeria monocytogenes, is believed to be driven by the polymerization of actin filaments [1–3]. By hijacking the actins of the host cell, these pathogens are able to form actin-rich comet tails behind them where propelling forces, large enough for their movements, are generated by the unidirectional polymerization of actin filaments [4]. It has been found that the only surface protein necessary for the Listeria motility is ActA [5]. Indeed, it has been demonstrated that microspheres coated with ActA can form actin comet tails and move in cytoplasmic extracts with speeds in the order of 0.1 μm/s [5,6]. Other cytoplasmic proteins that have been identified in participating the formation of comet tails include the Arp2/3 protein complex and the so called capping proteins. The Arp2/3 complex is believed to be able to bind to both ActA and actin filaments, and facilitate the nucleation of nascent filaments [7], whereas the capping proteins stop the growths of actin filaments by binding to their barbed ends [8].

Several mechanisms have been proposed to explain the force generation by polymerization. Maybe the most well-known one is the so called elastic Brownian ratchet (EBR) model [9,10], where the central idea is that the filament tip is able to fluctuate away from the load surface to allow the addition of new actin monomers. A force-velocity relationship is then obtained from a perturbation solution which is valid as long as the polymerization rate is small [10]. No interaction between the filament and the load surface was considered in the original EBR formulation. However, subsequent experiments, see [11,12], for example, have convincingly demonstrated that the actin comet tail is actually attached to the surface of Listeria or microsphere. To account for this important finding, Mogilner and Oster [13] presented a modified EBR model, where bonding between the actin filament and the ActA/Arp2/3 protein complex on the load surface was allowed. In the modified model, the filaments attached to the surface were treated differently from those that remain free. For free filaments, the force-velocity relationship drawn from the original EBR model was assumed to be valid, whereas descriptions concerning the enforced breaking of molecular bonds proposed by Bell [14,15] were directly applied to filaments attached to the load surface. Effectively, in this formulation, filaments adhered to the surface can only generate "frictional" forces opposing the movement of Listeria or bead.

On the basis of the original EBR formulation, here we present a different mechanics model for the force generation by polymerization. The possible bonding between the actin filament and the load surface is represented by an attractive interaction potential and hence all filaments are treated in a unified manner. This model is simple enough to allow essential results to be presented in closed forms yet it still takes into account several important features of actin-based motility, such as the nucleation and capping of filament tips. We hasten to point out that the validity of the solution to be presented here does not depend on the assumption that the polymerization rate is small, so the limitation in [10,13] is removed.

The rest of the paper is organized as follows. The generalized formulation describing the force generation by the Brownian motions of particles is presented in the following section. Then assumptions and descriptions suitable for cases involving actin polymerization are introduced and a closed form solution is provided. After that, model predictions are compared with recent experiment observations and the implications for understanding the enhanced actin-driven motility of Listeria and bead by the presence of Vasodilator-stimulated phosphoprotein (VASP) are discussed. Finally, concluding remarks and thoughts are provided.

II. GENERALIZED FORMULATION

Consider the Brownian motions of particles near a rigid wall. The word "particle" here may represent a molecule or, in a broader sense, any object that has the ability to diffuse. We put the origin of our reference frame on the surface of the wall so the distance between the wall and the diffusing particle is x, as depicted in Fig. 1. Assume the wall is moving with a speed V in the negative x direction and let $U(x)$ be the potential energy of a particle at position $x>0$, as schematically shown in Fig. 1. The behavior of the particle is characterized by the density of states, denoted by $p(x,t)$, which is the normalized probability distribution of a large ensemble of

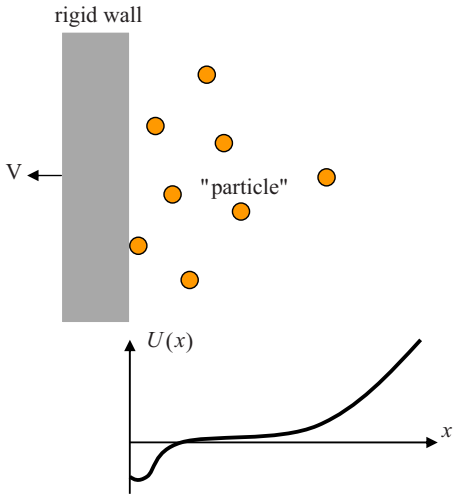

FIG. 1. (Color online) Schematic plot of the Brownian motions of particles near a wall. The potential energy of a particle at position x is represented by $U(x)$.

such "identical" particles. In the moving frame we chose, the evolution of the density of states is governed by the Smoluchowski equation as

$$\frac{\partial p}{\partial t} = D\frac{\partial^2 p}{\partial x^2} + D\frac{\partial}{\partial x}\left[\frac{\partial U/kT}{\partial x}p\right] + h(x,t) - V\frac{\partial p}{\partial x},$$

$$\text{for } 0 < x < \infty, \tag{1}$$

where kT is the thermal energy, D is the diffusion coefficient of particles, and h is the source (or sink) distribution representing the generation (or elimination) of particles. We are particularly interested in the steady state solution of Eq. (1). For a steady state solution to exist, h must be a function of x only, and the total number of particles is expected to be conserved, that is

$$\int_0^\infty h(x)dx + J(0) - J(\infty) = 0 \tag{2}$$

in which J is the probability flux defined as

$$J(x) = -\left[D\frac{dp}{dx} + D\frac{dU/kT}{dx}p - Vp\right]. \tag{3}$$

To evaluate the force generated by particles, assume the wall is actually "penetratable" with an energy penalty U_w defined as

$$U_w/kT = \tfrac{1}{2}K_w x^2 \tag{4}$$

associated with the penetration of a single particle to position $x<0$. Effectively, the wall is treated as a spring acting on particles in the region $x<0$. As the normalized spring constant K_w approaches infinity, the situation reduces to the limiting case where the wall is rigid. Under this condition, the steady state probability distribution $p(x)$ in the region $x<0$ is essentially governed by

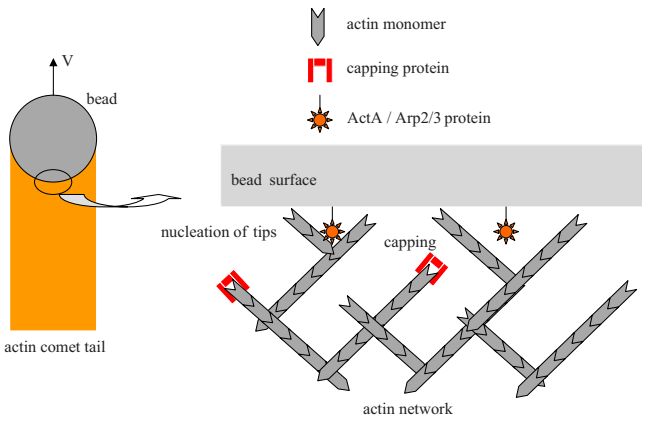

FIG. 2. (Color online) Schematic plot of the actin comet tail near the bead surface.

$$D\frac{d^2p}{dx^2} + D\frac{d}{dx}\left[\frac{d(U_w/kT)}{dx}p\right] = 0, \quad \text{for } x < 0, \tag{5}$$

where small terms, compared with U_w as $K_w \to \infty$, have been neglected. The magnitude of the propelling force (in the negative x direction) generated by a single particle can be calculated as

$$f = \frac{\int_{-\infty}^{0} (-dU_w/dx)p(x)dx}{\int_{-\infty}^{0} p(x)dx + \int_0^\infty p(x)dx}. \tag{6}$$

From Eqs. (4) and (5), it can be shown that the force f, as defined above, takes the simple form

$$f = kT\frac{p(0)}{\int_0^\infty p(x)dx}. \tag{7}$$

Now, the only remaining question is to find the density of states $p(x)$ as a solution of Eq. (1) subjected to proper form of the potential $U(x)$ and source distribution $h(x)$, as well as proper boundary conditions, which are determined by the specific nature of the problem one wants to examine.

III. ACTIN-BASED MOTILITY

Beads coated with ActA proteins have been found to propel themselves by forming actin comet tails behind them [5]. The dendritic structure of actin filaments in the comet tail [6] is thought to be formed by the branching of nascent filaments from the sides of existing ones. This nucleation process is facilitated by the so called Arp2/3 complex which can bind to both ActA and actin [16]. In contrast to the nucleation of new tips, some actin filaments lose the ability to grow due to the binding of capping proteins to their barbed ends [7]. All the features mentioned above are schematically shown in Fig. 2.

Theoretically, the actin-driven motility of beads or Listeria monocytogenes has been studied by Mogilner and Oster

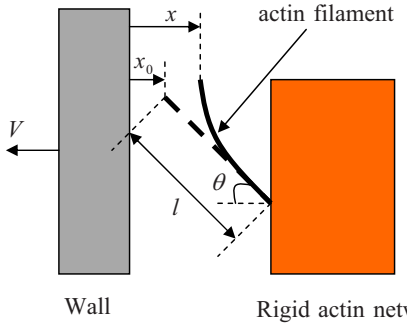

FIG. 3. (Color online) Configurations of actin filament. The dashed line represents the undeformed filament and the solid line corresponds to the deformed one.

[10,13]. The central idea behind their models is that the thermal excitation is large enough to bend the actin filament and create a gap between the tip and the load surface which allows polymerization to happen. A propelling force, large enough for the movement of bead or Listeria monocytogene, will then be generated as a result of this continuous polymerization. Based on a similar approach, here we re-examine the problem in the framework as described in the previous section. In this case, the particles appearing in Fig. 1 represent the actual tips of actin filaments.

A. Determination of $U(x)$

To formulate the problem, the form of U, as appears in Eq. (1), needs to be determined first. We proceed by decomposing $U(x)$ into two parts as

$$U(x) = U_b(x) + U_i(x), \tag{8}$$

where U_b represents the bending energy stored in the filament and U_i accounts for the interaction energy between the load surface and the tip. Following [10], we assume that each filament has the same free end length l and all filaments run into the wall with the same angle θ, as shown in Fig. 3.

By treating the actin fibers as cantilever beams, the bending energy stored in each filament can be written as

$$U_b(x) = \frac{1}{2}K_f(x - x_0)^2, \tag{9}$$

where x_0 is the tip position in the undeformed configuration, see Fig. 3, and K_f is the effective spring constant of filaments which takes the form [10,17]

$$K_f = \frac{3\lambda kT}{l^3 \sin^2 \theta} \tag{10}$$

in which λ is the so called persistence length of actin. As shown in Fig. 2, actin filaments can adhere to the load surface by forming bonds with ActA/Arp2/3 protein complex. A potential well U_i near the wall is introduced here to account for the possible adhesions between the tips and the wall. A specific form of U_i, suitable for current study, is chosen as

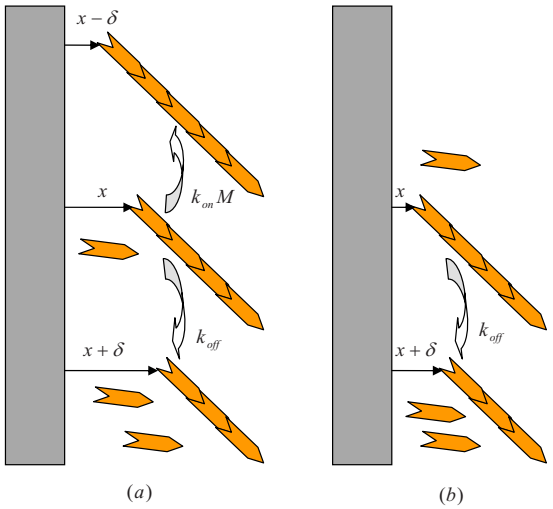

FIG. 4. (Color online) Transitions of tip position due to polymerization and depolymerization. (a) Both polymerization and depolymerization are admissible when the gap between the tip and the wall exceeds the projected size of a monomer δ. (b) When the gap between the tip and the wall is smaller than δ, only depolymerization is admissible.

$$U_i(x) = -C_b kT e^{-(x/\sigma)^2}, \tag{11}$$

where the parameter C_b has the physical meaning of the depth of the potential well and σ represents the approximate width of the well. Notice that the choice of Eq. (11) is somewhat arbitrary, however, from basic physics we know that depth and width are the two most important properties of any potential well. So as long as these two key quantities are fixed, the specific shape of the well should not affect the results significantly, similar to the enforced breaking of a molecular bond as discussed in [15]. It can easily be shown that the expression of the propelling force f, generated by a single filament, in this case takes a slightly different form,

$$f = kT\frac{p(0)}{\int_0^\infty p(x)dx} - \frac{\int_0^\infty p(x)(dU_i/dx)dx}{\int_0^\infty p(x)dx}, \tag{12}$$

where the first term on the right hand side comes directly from Eq. (7) and the second term represents the force generated by the attractive interaction between the filament tip and the wall.

B. Polymerization, nucleation, and capping of actin filaments

The transitions of tip position due to possible polymerization and depolymerization are schematically shown in Fig. 4. Basically, if the gap between the wall and the polymer tip exceeds the projected actin monomer size δ then a monomer can polymerize onto the tip with a rate (probability per unit time) $k_{on}M$, where k_{on} is the so called association rate for polymerization and M is the actin monomer concentration around the tip. Notice that here $\delta = \delta_0 \cos\theta$, where δ_0 is the actually size of an actin monomer. Polymerization is impos-

sible if the distance between the wall and the tip is less than δ. On the other hand, regardless of the tip position, a monomer can dissociate from the tip with a rate (probability per unit time) k_{off}. Polymerization will cause a tip to change its position from x to $x-\delta$, whereas the tip position jumps from x to $x+\delta$ after the dissociation of a single monomer. Based on these observations, the effects of polymerization and depolymerization can be represented by a source distribution h_p of the form

$$h_p(x) = k_{on}Mp(x+\delta) - k_{off}p(x), \quad \text{for } 0 < x < \delta \tag{13}$$

and

$$h_p(x) = k_{on}M[p(x+\delta) - p(x)] - k_{off}[p(x) - p(x-\delta)],$$

$$\text{for } x > \delta. \tag{14}$$

To derive the main results to be presented in the simplest way, the nucleation of new tips, facilitated by the Arp2/3 complex, is assumed to take place only on the load surface and hence it can be represented by a net probability flux J_0 at $x=0$, that is

$$J(0) = -\left[D\frac{dp}{dx} + D\frac{dU/kT}{dx}p - Vp\right]_{x=0} = J_0. \tag{15}$$

To describe the capping of tips when they are away from the load surface, a sink distribution h_c is also introduced here which takes the form

$$h_c(x) = -\frac{J_0}{\Delta}e^{(\delta-x)/\Delta}, \quad \text{for } x > \delta \tag{16}$$

and

$$h_c(x) = 0, \quad \text{for } 0 < x < \delta, \tag{17}$$

where Δ is a parameter describing the approximate size of the region where capping reactions take place. The total source distribution h, as appears in Eq. (1), is just the superposition of h_p and h_c introduced above, that is

$$h(x) = h_p(x) + h_c(x). \tag{18}$$

Notice that the potential energy U is unbounded as $x \to \infty$, see Eq. (9), so we expect the flux $J(x)$, as well as the density of states $p(x)$, to vanish as x approaches infinity. It can then be verified that the conservation condition (2) is indeed satisfied. We must point out that the simple treatments of the nucleation and capping of tips adopted here are for the purpose of illustration only. However, we do believe that the main features of the problem have been included in this simple description and, furthermore, more realistic and complicated treatments can easily be incorporated into the formulation presented here, if necessary.

IV. GENERAL SOLUTIONS

In most practical cases, polymerization is much faster than depolymerization, so we proceed by neglecting the possible dissociation reactions in our formulation. In addition, we replace the term $p(x+\delta)-p(x)$ with $\delta\frac{dp}{dx}$ in Eq. (14), and $p(x+\delta)$ with $p(\delta)$ in Eq. (13), respectively. These approximations are valid as long as $\delta^2|dp/dx| \ll 1$, meaning that the probability distribution varies slowly on the length scale of a monomer size δ. Nondimensionlize the problem as follows:

$$\hat{p} = p\delta, \quad s = x/\delta, \quad s_0 = x_0/\delta, \quad k_f = \frac{K_f\delta^2}{kT}, \quad u = U/kT,$$

$$\alpha = \frac{k_{on}M\delta^2}{D}, \quad \upsilon = \frac{V\delta}{D}, \quad \hat{\sigma} = \sigma/\delta, \quad \hat{\Delta} = \Delta/\delta, \quad j_0 = \frac{J_0\delta^2}{D}. \tag{19}$$

The governing equations then become

$$\frac{d^2\hat{p}(s)}{ds^2} + \frac{d}{ds}\left[\frac{du(s)}{ds}\hat{p}(s)\right] + \alpha\hat{p}(1) - \upsilon\frac{d\hat{p}(s)}{ds} = 0,$$

$$\text{for } 0 < s < 1 \tag{20}$$

and

$$\frac{d^2\hat{p}(s)}{ds^2} + \frac{d}{ds}\left[\frac{du(s)}{ds}p(s)\right] + \alpha\frac{d\hat{p}(s)}{ds} - \frac{j_0}{\hat{\Delta}}e^{(1-s)/\hat{\Delta}} - \upsilon\frac{d\hat{p}(s)}{ds} = 0,$$

$$\text{for } s > 1, \tag{21}$$

where

$$u(s) = k_f(s-s_0)^2/2 - C_b e^{-(s/\hat{\sigma})^2}. \tag{22}$$

The general solution, satisfying the boundary condition (15) as well as the continuity conditions at $s=1$, can be found as

$$\hat{p}(s) = e^{-u(s)+\upsilon s}\left[Ce^{-\alpha} + \int_s^1 [\alpha\hat{p}(1)q + j_0]e^{u(q)-\upsilon q}dq\right],$$

$$\text{for } 0 < s < 1, \tag{23}$$

and

$$\hat{p}(s) = e^{-u(s)-(\alpha-\upsilon)s}\left[C - j_0\int_1^s e^{(1-q)/\hat{\Delta}}e^{u(q)+(\alpha-\upsilon)q}dq\right],$$

$$\text{for } s > 1, \tag{24}$$

where C is a constant. At steady state, the velocity V must be defined in a self-consistent manner as

$$V = k_{on}M\delta\frac{\int_\delta^\infty p(x)dx}{\int_0^\infty p(x)dx}. \tag{25}$$

For any given values of V, Eq. (25) and the normalization condition

$$\int_0^\infty p(x)dx = 1 \tag{26}$$

provide us two equations that can be used to determine the two constants C and s_0 appearing in the general solution. With a closed form solution at hand, the propelling force f, corresponding to velocity V, can be determined through Eq. (12).

V. RESULTS AND DISCUSSIONS

Before presenting any results, the values of a set of parameters must be chosen first. The effective monomer size δ_0 of actin is about 2.7 nm [18], and the persistence length λ of actin filaments has been measured to be around 10 μm [19]. Experiment observations suggest that the length of actin filaments in the comet tail is in the order of 100 nm [6], usually the long filaments are predominantly parallel to the moving direction and cross linked by randomly oriented short ones [8]. Here we estimate that the free end length of filaments l varies from 60 to 200 nm. Arp2/3 branches filaments at about 70° [6], so the angle θ is chosen to be 35° here. The normalized effective spring constant of filaments k_f is estimated to be within the range of 0.05–2.

Getting an estimate on the diffusion coefficient D of actin tips is more difficult. From the Einstein relation, D relates to viscous drag coefficient ξ through $D=kT/\xi$. If the filament is treated approximately as an ellipsoid with major axis $l/2$ and minor axis b, where $b\approx 4$ nm is the radius of the actin fiber [20], then we have $\xi=4\pi\eta l/[\ln\frac{l}{b}+1/2]$ with η being the viscosity of the environment. The value of η varies from 0.03 P for the fluid component of cytoplasm to 30 P for the cytoplasm itself [21]. Hence the tip diffusivity D is estimated to vary from 0.002 to 2 $\mu m^2/s$. The value of $k_{on}M$ is believed to be in the order of 100 s^{-1} [18]. Based on these observations, the normalized polymerization rate α is estimated to be within the range of 3.5×10^{-4}–0.35.

The width of the potential well σ depends on the nature of the bond formed between actin filament and ActA/Arp2/3 complex, however, it is reasonable to believe that its value is within the range of 0.1–1 nm. The values of all parameters used here are gathered in Table I.

Choosing $j_0=0$, i.e., there is no nucleation or capping of filament tips, the force-velocity relationships corresponding to $C_b=0$, 2, and 3 are shown in Fig. 5. Clearly, the velocity V decreases monotonically as the propelling force f increases. Recall that C_bkT is the depth of the potential well, so C_b represents the adhesion strength between the tip and the wall. From Fig. 5, it is obvious that the presence of attractive interactions between the tip and the wall reduces the force generation capability of filaments. This is not surprising because, in order for polymerization to take place, the tip must fluctuate away from the wall which, clearly, is opposed by the attractive interactions between them.

Influences of the nucleation (or capping) rate of tips on the polymerization-driven motility can be examined by our model as well. Choosing $C_b=1$, the force-velocity relationships for different j_0 values are illustrated in Fig. 6, which showed that the force generation ability of filaments is lowered by the nucleation and capping of tips. This reduction is significant in the high load regime, where the propelling force is large and the velocity is small, and becomes negligible in the regime where the load is small; see Fig. 6. The negative impact of the nucleation and capping of tips on the force generation by polymerization is not unexpected; only those filaments with tips away from the wall can polymerize and, obviously, the number of such filaments is reduced by the capping reactions.

TABLE I. Parameter values.

Notation	Meaning	Value
δ_0	effective actin monomer size	2.7 nm
θ	inclined angle between the actin filament and the wall	35°
λ	persistence length of actin filament	10 μm
$k_{on}M$	polymerization rate	100 s^{-1}
σ	approximate width of the potential well	0.22 nm
Δ	approximate size of the region where capping reactions take place	4.4 nm
α	dimensionless polymerization rate	0.02
k_f	normalized effective spring constant of filaments	1

Once the force-velocity relationship is obtained, the moving velocity of the bead V_b can be determined through the Stokes relation

$$f = \frac{6\pi a\eta}{N}V_b = \beta V_b, \tag{27}$$

where N is the total number of filaments behind the bead, a is the radius of the bead, and η is the viscosity. The relationship between f and V_b as shown in Eq. (27) is represented by the dashed line in Fig. 5, and the intersection point between this line and the force-velocity curve of filaments provides the actual moving velocity of the bead. If the spacing between filaments is chosen as 100 nm then $N\approx 25$ for a bead with diameter of 0.5 μm. Choosing $j_0=0.1$ and $\eta=30$ P, the

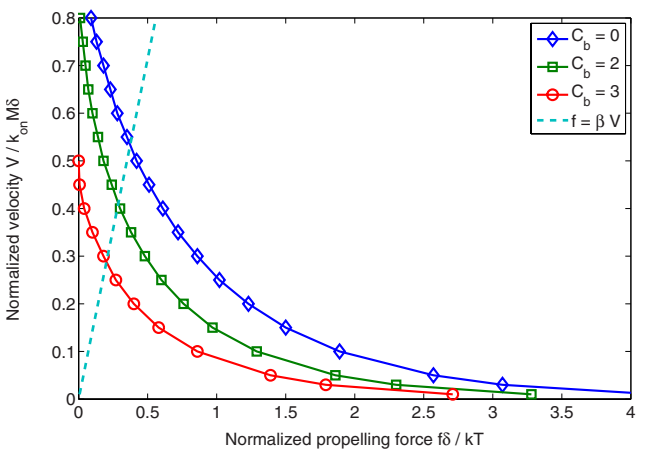

FIG. 5. (Color online) The force-velocity relationship under different adhesion strength conditions.

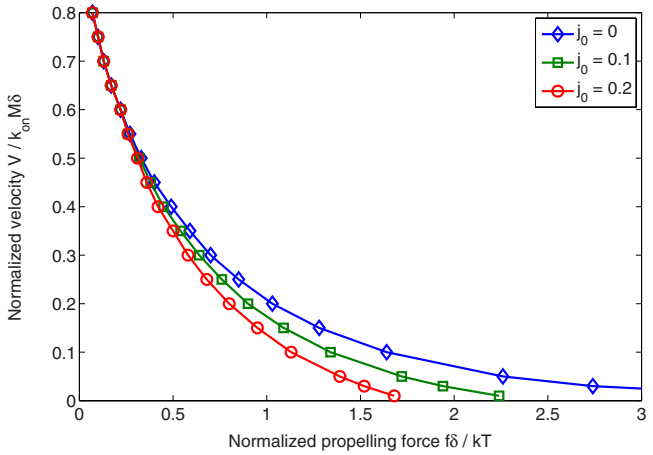

FIG. 6. (Color online) The force-velocity relationship under different tip nucleation and capping rates.

same viscosity as the cytoplasm, the bead velocity as a function of the adhesion strength between the tip and the surface is shown in Fig. 7. Clearly, as expected, the bead velocity drops as the adhesion strength increases. The bead speed predicted here is in the order of 0.1 μm/s which agrees with the observations by Cameron *et al.* [6].

The vasodilator-stimulated phosphoprotein (VASP) has been found to enhance the actin-based motility of Listeria or bead [7,22]. Samarin *et al.* [7] suggested that VASP increases the dissociation rate between actin filaments and ActA/Arp2/3 complex by a factor of about 100. From thermodynamics, we know that the dissociation rate is proportional to e^{-C_b}, so the presence of VASP can be represented by a decrease in the value of C_b in our model. From Fig. 7, it can be seen that as the value of C_b drops from 4 to 0, corresponding to a 50-fold increase in the dissociation rate, the bead velocity roughly grows by a factor of 10 which is comparable to experiment observations [7,22].

The sensitivity of the other two key parameters used in the model, namely the effective spring constant of filaments k_f and the approximate width of the potential well σ, has been investigated as well. In all the calculations presented above, the values of these two parameters are chosen as

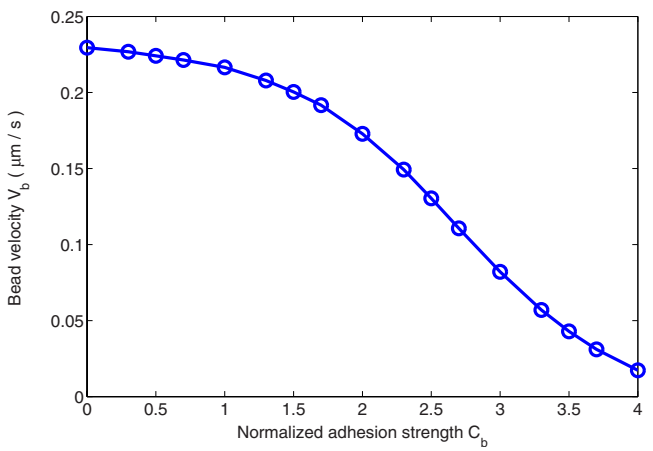

FIG. 7. (Color online) Bead velocity as a function the adhesion strength between the tip and the bead surface.

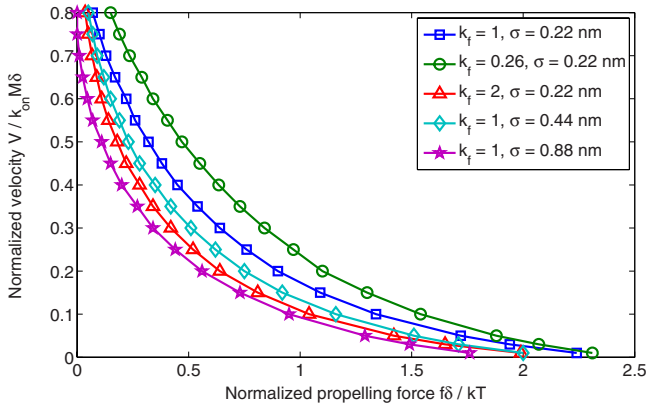

FIG. 8. (Color online) The force-velocity relationships corresponding to different spring constants of filaments, as well as different potential well depths.

σ=0.22 nm and k_f=1. As mentioned earlier, the width of the potential well is expected to be within the range of 0.1–1 nm, whereas k_f is estimated to vary from 0.26 to 2, corresponding to filaments with free end length of 120 and 60 nm, respectively. Choosing C_b=1 and j_0=0.1, model predictions corresponding to different values of σ and k_f are shown in Fig. 8, where it is clear that, as expected, the force generation by polymerization is reduced when the attractive interaction between the tip and the load surface has a longer influence range, i.e., larger value of σ. Figure 8 also demonstrated that softer filaments, i.e., with longer free end length, have better force generation capabilities. Again, this is not surprising because longer filament has lower bending resistance and hence a gap between the tip and the load surface, necessary for polymerization to take place, is more likely to be created by thermal excitations. Another important observation from Fig. 8 is that although model predictions depend on the specific values of parameters we choose, they all fall within the same order of magnitude. This leads us to believe that the two conclusions drawn from the model, namely that a bead speed around 0.1 μm/s can be achieved by actin polymerization and an approximate ten-fold increase in velocity can be induced by the presence of VASP, should be rather robust.

To further test our model, we have also compared its predictions to two sets of experimental data reported by McGrath *et al.* [23] and Marcy *et al.* [24], respectively. By varying the viscosity of the fluid, McGrath and co-workers obtained the force-velocity relationship for the actin-based motility of Listeria monocytogenes, as represented by the filled circular symbols in Fig. 9 [23]. If we assume that there are 22 actin filaments behind Listeria, which corresponds to an average filament spacing of around 100 nm for Listeria monocytogene with diameter of 0.5 μm, the model prediction by choosing C_b=2, k_f=1, j_0=0.01, σ=0.22 nm, Δ=4.4 nm, and $\delta k_{on} M$=80 nm/s is represented by the solid line in Fig. 9. Clearly, the main features of the experiment observations have been captured by the model.

In another set of experiment conducted by Marcy and co-workers [24], the force-velocity relationship for a 2.1-μm polystyrene bead driven by actin comet tail was measured by gluing the bead to a flexible fiber and holding the comet tail

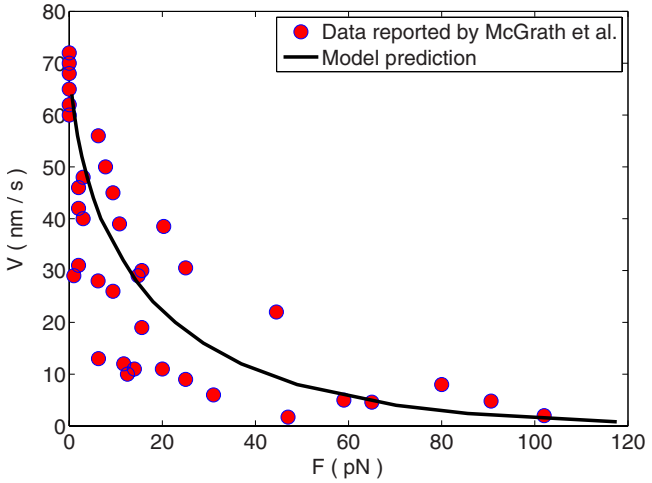

FIG. 9. (Color online) Comparison between the model prediction and the experimental data reported by McGrath *et al.* [23].

with a micropipette. The data are represented in Fig. 10 by the filled square symbols. The bead velocity as shown in Fig. 10 was normalized by its value when the external force is zero, i.e., $V_{(F=0)}$. A negative force in Fig. 10 means that the loading direction and the moving direction of bead are identical. Notice that the total force acting on the bead can be as large as several nano-Newtons (nN), which seems to suggest that several thousand filaments are in the comet tail because the force scale of a single filament is in the order of 2 pN, i.e., $kT/\delta \sim 2$ pN. Choosing the number of working filaments as 2600, corresponding to a filament spacing of around 40 nm, and other parameters as $C_b=3$, $k_f=1$, $j_0=0.01$, $\sigma=0.44$ nm, and $\Delta=4.4$ nm, the model prediction is illustrated in Fig. 10 by the solid line. Again, the model prediction compares favorably with the experimental data.

At this point, it is informative to compare the formulation presented here with other existing models. Here, the well-known modified EBR model [13] is chosen to serve this purpose because, to our knowledge, it is the only quantitative model available in the literature that takes into account the

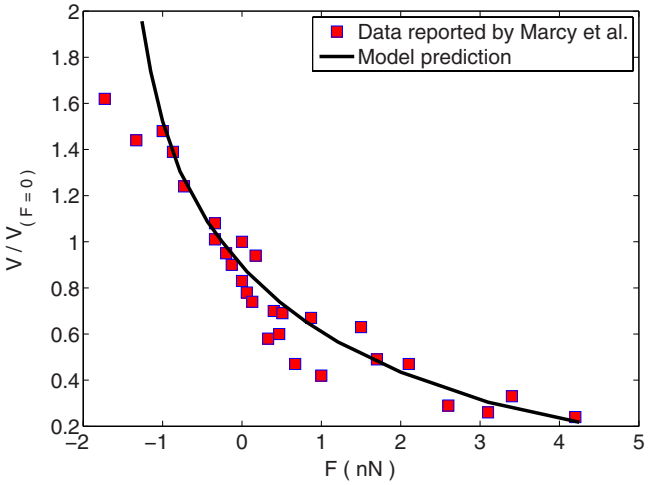

FIG. 10. (Color online) Comparison between the model prediction and the experimental data reported by Marcy *et al.* [24].

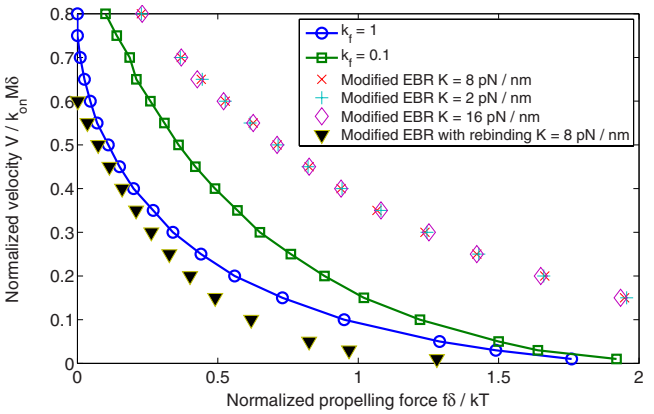

FIG. 11. (Color online) Comparison of the predictions from the present model with those from the modified EBR model.

adhesions between the filaments and the load surface. Detailed formulation of this model is given in the Appendix; basically the filaments are divided into two groups, namely the attached filaments that adhere to the load surface and the free filaments that remain unattached. The force generation capability of free filaments is assumed to be described by the force-velocity relationship drawn from the original EBR model [10], whereas the force-dissociation relationship, describing the enforced breaking of molecular bonds, proposed by Bell [14] is applied to attached filaments. Choosing $C_b=1$, $j_0=0.1$, and $\sigma=0.88$ nm, the predictions from our model corresponding to $k_f=0.1$ and 1 are plotted in Fig. 11 in comparison with those from the modified ERB formulation. Notice that, in contrast to our predictions, results from the modified EBR model are independent of k_f because this parameter does not appear in the model formulation at all; see the Appendix.

An immediate observation from Fig. 11 is that the results obtained from the modified EBR model deviate a lot from our predictions. Figure 11 also clearly showed that the predictions from the modified EBR model are insensitive to the parameter K, which is the effective spring constant of the bond formed between filament tip and load surface.

Several factors may contribute to the large differences between our predictions and those from the modified EBR model. First of all, as pointed out in the Appendix, the possibility of the rebinding of free filaments to load surface is neglected in the modified EBR formulation, consequently, the population of free filaments will be overpredicted. This may explain the overpredictions of the force generation capability by polymerization from the modified EBR model in comparison with our results. We have tried to correct this by adding a rebinding term to the modified EBR formulation, see the Appendix, and the results are also shown in Fig. 9. Clearly, the possibility of rebinding significantly lowers the force generation capability of filaments, and the predictions by including rebinding are much closer to our results corresponding to $k_f=1$. Instead of considering the association and dissociation reactions and making assumptions on the kinetics associated with them, we directly consider the Brownian motions of filament tips in a potential field in our formulation and hence all the "breaking" and "rebinding" issues

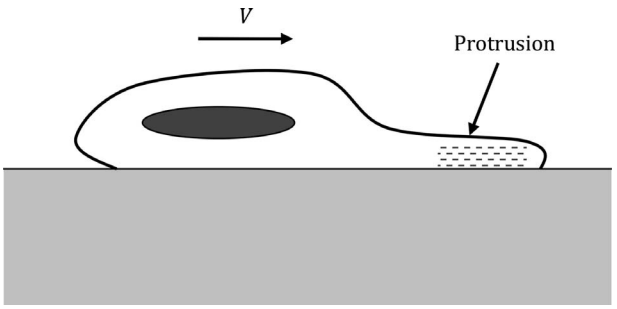

FIG. 12. Schematic plot of a locomoting cell with protrusion formed at its leading edge.

have been inherently taken care of. In this regard, we feel that the predictions from our model should be more accurate. It is also necessary to point out that the force-velocity relationship (A5) is valid only under limiting conditions where the propelling force is large [10], i.e., $f/K_f\delta \gg 1$. However, it is obvious that this condition is not strictly satisfied within the range of calculations as shown in Fig. 9, and this may explain the discrepancies between our predictions and those from the modified EBR model as well. Lastly, the so called Bell's relation (A3), describing the dissociation of a molecular bond under constant force, is accurate only when the potential energy profile of the bond has a sharp barrier at a fixed position σ along the dissociation pathway [15], which obviously is not the case here; see Eq. (11).

The discussions so far have been mainly focusing on the actin-based motility of bead or Listeria, however, we believe that the model presented here can be used directly in studying actin networks elsewhere. In cell locomotion, for example, a so called protrusion region will usually be formed at the leading edge of motile cells, as schematically shown in Fig. 12. The formation of protrusion at the leading edge, stabilization of this region by adhesion, and the retraction of the trailing edge constitute the cycle of cell movement. It is well known that actin polymerization inside the cell is responsible for the formation of such protrusions [25,26], hence our model should be useful in analyzing this process as well. In this case the force generated by actin polymerization must be large enough to overcome the membrane tension that prevents the formation of protrusions.

In our opinion, several features of the model presented here make it advantageous in analyzing actin-driven phenomena under certain conditions. First of all, unlike many other models in the literature, the validity of our model does not depend on the assumption that the polymerization rate is small, which may be highly desirable in certain situations. For example, keratocytes have the amazing ability to move with a speed up to 1 μm/s [27], in this case the normalized velocity v appeared in Eq. (19) is estimated to be in the order of 0.1, a moderate value. Under this condition, it is unclear whether models based on perturbation solutions under small velocity assumption, like those presented in [10,13], can be directly used and expected to yield accurate predictions. Second, when compared with other models, like the modified EBR formulation discussed above, the use of our model also seems to be less restricted by conditions such as the magnitude of load and the shape of the interaction potential between filaments and load surface. Finally, we feel that the formulation presented here provides us a unified framework for examining, in great detail, the influences of different factors on the force generation by polymerization. For instance, although this model is aimed to consider the adhesions between the filaments and the load surface, there is no difficulty in applying it to situations where the interactions between them are repulsive. In a broader sense, our model can be applied to other biological, chemical, or physical systems where Brownian motions are utilized to generate propelling forces. In this bigger picture, the generalized formulation presented here is fully capable of dealing with situations where particles interact with each other, a typical example being that the particles are charged. In this case, the potential field U depends on the density of states $p(x)$ and the problem must be solved in a self-consistent manner.

VI. CONCLUDING REMARKS

On the basis of the well-known elastic-Brownian ratchet mechanism on force generation by polymerization [9,10], a different model is developed here to study the influence of the possible adhesions between the actin filaments and the load surface, as well as the nucleation and capping of filament tips, on actin-based motility. An attractive interaction potential is introduced to account for the possible bonding between the actin filament tip and the ActA/Arp2/3 complex on the load surface [7]. The possible nucleation of tips is represented by a probability flux at the boundary, whereas the capping is described by a distributed sink of tips.

A closed form solution is obtained from the formulation which remains valid even when the polymerization rate is high. By collecting the parameter values from the literature and reasonable estimation, the velocity of a bead, driven by actin polymerization, is estimated and the value ($\sim$0.1 μm/s) is consistent with experiment observations [6]. Our model predicts an increase in bead velocity as the adhesion between the tip and the bead surface becomes weaker. We believe this has deeper implications for understanding the enhanced bead motility by the presence of VASP, as observed in recent experiments [7]. It is suggested that VASP greatly increases the dissociation rate between the actin filaments and the ActA/Arp2/3 complex on bead surface, which indicates that the presence of VASP weakens the adhesion between the tip and the surface and consequently, according to our model, enhances the bead motility.

Several simplifications have been made here to facilitate the analyses. For one thing, the diffusivity of newly nucleated tips is assumed to be the same as that of old ones. Strictly speaking, this may not be true and more realistic treatments, based on the actual structure of the branched network of filaments, are required in the future to address this issue. For another, it is assumed that any filament tip can polymerize, whenever possible, with a constant rate $k_{on}M$, which is a significant simplification of what happened in real situations. During the formation of protrusion, for example, a spatial gradient of the association (or dissociation) rate for polymerization will be created by a cell to enforce the continuous addition of actin monomers to the barbed ends of

filaments, as well as the dissociation of actins at the opposite ends. In addition, to sustain the continuous movement, actins also need to be transported from the interior of the cell to the front edge of the protrusion. So the force generation by actin polymerization is likely to be regulated by the active behaviors of cells in a much more complicated manner than what has been considered here.

We must also point out that there are other alternative hypotheses on the force generation mechanism in the literature, such as the molecular motor based end-tracking model [17,28]. It is hard to tell, from experiment data available, which mechanism is actually responsible for the generation of propelling force by actin polymerization and more carefully designed measurements are needed in the future to serve this purpose. Recently, by analyzing the trajectories of moving Listeria monocytogenes, Shenoy and co-workers suggested that a torque, besides the propelling force, should be generated by the actin comet tail as well [29]. To us, this seems to imply the generation of shear forces, parallel to the load surface, by actin polymerization. This issue is beyond the scope of this paper and is left for future studies.

ACKNOWLEDGMENTS

This investigation was supported by the Seed Funding Programme for Basic Research from The University of Hong Kong (Project No. 200809159003).

APPENDIX

In the modified EBR model developed by Mogilner and Oster [13], the filaments are divided into two groups, namely the attached filaments that adhere to the load surface and the free filaments that remain unattached. Denote n_a and n_w, $n_a+n_w=1$, as the fractions of filaments of these two groups, respectively. If a frictional force f_a is generated by an attached filament, whereas a propelling force f_w is generated by a free filament, then the average propelling force generated by a single filament is

$$f = -n_a f_a + n_w f_w. \tag{A1}$$

At steady state, n_a and n_w are constants, that is

$$\frac{dn_a}{dt} = J_0 - k_- n_a = 0, \quad \frac{dn_w}{dt} = k_- n_a - J_0 = 0, \tag{A2}$$

where, as introduced earlier, J_0 is the nucleation, as well as the capping, rate of filament tips. k_- is the so called dissociation rate which, according to the famous Bell's relation [14], takes the form

$$k_- = k_-^0 e^{f_a \sigma/kT} = k_-^0 e^{f_a/f_b}. \tag{A3}$$

Here, σ is the width of the potential well describing the attractive interaction between the tip and the load surface, and $f_b=kT/\sigma$. From thermodynamics, the constant k_-^0, representing the escape rate of filament tips from a potential well with width σ and depth C_bkT, can be approximately expressed as

$$k_-^0 = \frac{2D}{\sigma^2} e^{-C_b}, \tag{A4}$$

where, again, D is the diffusion coefficient of filament tips. The force-velocity relationship drawn from the original EBR model [10], neglecting depolymerization, is directly applied to the free filaments here, that is

$$V = V_{\max} e^{-f_w \delta/kT}. \tag{A5}$$

Here, $V_{\max}=k_{on}\delta M$ is the free polymerization velocity. Mogilner and Oster [13] further assumed that the bonds formed between filaments and load surface behave like linear springs, with spring constant K, so the dissociation rate k_- for filaments that remain attached to the surface after time t is

$$k_- = k_-^0 e^{VtK/f_b} \tag{A6}$$

from which the average life time for an attached filament can be calculated as [13]

$$\langle t \rangle = \int_0^\infty t k_-^0 e^{VtK/f_b} \exp\left[-\frac{k_-^0 f_b}{KV} (e^{VtK/f_b} - 1) \right] dt. \tag{A7}$$

The average frictional force f_a, generated by a single attached filament, hence takes the form

$$f_a = KV\langle t \rangle. \tag{A8}$$

The fraction n_a can then be determined from Eq. (A8) and (A2) as

$$n_a = \frac{J_0}{k_-^0} e^{-KV\langle t \rangle/f_b}. \tag{A9}$$

Equations (A7)–(A9), (A1), and (A5) constitute a self-consistent mathematical system from which the force-velocity relationship can be drawn numerically. Here, the calculations are conducted by choosing $C_b=1$, $j_0=1$, $\sigma=0.88$ nm, and other parameter values as listed in Table I. The spring constant K is estimated from the following relationship:

$$K = \frac{2C_b}{\sigma^2} kT, \tag{A10}$$

which basically means that the depth of the potential well should equal to the energy stored in the spring when stretched to a distance identical to the width of the well. Based on the parameters we choose, K is estimated to be around 8 pN/nm. We have also conducted calculations by choosing $K=2$ pN/nm and $K=16$ pN/nm, and it seems that the model predictions are insensitive to this parameter; see Fig. 9.

Notice that the possibility of the rebinding of free filaments to load surface is neglected in Eq. (A2), consequently, the population of free filaments will likely be overpredicted. To correct this, we add a rebinding term to Eq. (A2) as

$$\frac{dn_a}{dt} = J_0 - k_- n_a + k_+ n_w = 0, \quad \frac{dn_w}{dt} = k_- n_a - J_0 - k_+ n_w = 0, \tag{A11}$$

where k_+ is the so called association rate, which is expected to be a constant and takes the following form:

$$k_+ = \frac{2D}{\sigma^2}. \tag{A12}$$

In this case, the expression of n_a becomes

$$n_a = \frac{J_0 + k_+}{k_-^0 e^{KV\langle t\rangle/f_b} + k_+}. \tag{A13}$$

[1] J. M. Sanger, J. W. Sanger, and F. S. Southwick, Infect. Immun. **60**, 3609 (1992).
[2] J. A. Theriot, T. J. Mitchison, L. G. Tilney, and D. A. Portnoy, Nature (London) **357**, 257 (1992).
[3] T. P. Loisel, R. Boujemaa, D. Pantaloni, and M.-F. Carlier, Nature (London) **401**, 613 (1999).
[4] L. G. Tilney and D. A. Portnoy, J. Cell Biol. **109**, 1597 (1989).
[5] L. A. Cameron, M. J. Footer, A. van Oudenaarden, and J. A. Theriot, Proc. Natl. Acad. Sci. U.S.A. **96**, 4908 (1999).
[6] L. A. Cameron, T. M. Svitkina, D. Vignjevic, J. A. Theriot, and G. G. Borisy, Curr. Biol. **11**, 130 (2001).
[7] S. Samarin, S. Romero, C. Kocks, D. Didry, D. Pantaloni, and M-F. Carlier, J. Cell Biol. **163**, 131 (2003).
[8] A. S. Sechi, J. Wehland, and J. V. Small, J. Cell Biol. **137**, 155 (1997).
[9] C. S. Peskin, G. M. Odell, and G. F. Oster, Biophys. J. **65**, 316 (1993).
[10] A. Mogilner and G. Oster, Biophys. J. **71**, 3030 (1996).
[11] S. C. Kuo and J. L. McGrath, Nature (London) **407**, 1026 (2000).
[12] F. Gerbal, V. Laurent, A. Ott, M-F. Carlier, P. Chaikin, and J. Prost, Eur. Biophys. J. **29**, 134 (2000).
[13] A. Mogilner and G. Oster, Biophys. J. **84**, 1591 (2003).
[14] G. I. Bell, Science **200**, 618 (1978).
[15] E. Evans and K. Ritchie, Biophys. J. **76**, 2439 (1999).
[16] R. Boujemaa-Paterski, E. Gouin, G. Hansen, S. Samarin, C. L. Clainche, D. Didry, P. Dehoux, P. Cossart, C. Kocks, M-F. Carlier, and D. Pantaloni, Biochemistry **40**, 11390 (2001).
[17] R. B. Dickinson, L. Caro, and D. L. Purich, Biophys. J. **87**, 2838 (2004).
[18] T. Pollard, J. Cell Biol. **103**, 2747 (1986).
[19] D. Boal, *Mechanics of the Cell* (Cambridge University, Cambridge, England, 2002).
[20] A. Bremer, R. C. Millonig, R. Sutterlin, A. Engel, T. D. Pollard, and U. Aebi, J. Cell Biol. **115**, 689 (1991).
[21] M. Dembo, Biophys. J. **55**, 1053 (1989).
[22] V. Laurent, T. P. Loisel, B. Harbeck, A. Wehman, L. Gröbe, B. M. Jockusch, J. Wehland, F. B. Gertler, and M-F. Carlier, J. Cell Biol. **144**, 1245 (1999).
[23] J. L. McGrath, N. J. Eungdamrong, C. I. Fisher, F. Peng, L. Mahadevan, T. J. Mitchison, and S. C. Kuo, Curr. Biol. **13**, 329 (2003).
[24] Y. Marcy, J. Prost, M-F. Carlier, and C. Sykes, Proc. Natl. Acad. Sci. U.S.A. **101**, 5992 (2004).
[25] J. A. Theriot and T. J. Mitchison, Nature (London) **352**, 126 (1991).
[26] J. V. Small, Semin. Cell Biol. **5**, 157 (1994).
[27] E. de Beus and K. Jacobson, Cell Motil. Cytoskeleton **41**, 126 (1998).
[28] R. B. Dickinson and D. L. Purich, Biophys. J. **82**, 605 (2002).
[29] V. B. Shenoy, D. T. Tambe, A. Prasad, and J. A. Theriot, Proc. Natl. Acad. Sci. U.S.A. **104**, 8229 (2007).